

A Multiple Impact Origin for the Moon

Raluca Rufu^{1*}, Oded Aharonson¹, Hagai B. Perets²

¹Weizmann Institute of Science, Department of Earth and Planetary Sciences, Rehovot 76100, Israel.

²Technion Israel Institute of Technology, Physics Department, Haifa 32000, Israel.

*Contact Information: e-mail: Raluca.rufu@weizmann.ac.il

The hypothesis of lunar origin by a single giant impact can explain some aspects of the Earth-Moon system. However, it is difficult to reconcile giant impact models with the compositional similarity of the Earth and Moon without violating angular momentum constraints. Furthermore, successful giant impact scenarios require very specific conditions such that they have a low probability of occurring. Here we present numerical simulations suggesting that the Moon could instead be the product of a succession of a variety of smaller collisions. In this scenario, each collision forms a debris disk around the proto-Earth that then accretes to form a moonlet. The moonlets tidally advance outward, and may coalesce to form the Moon. We find that sub-lunar moonlets are a common result of impacts expected onto the proto-Earth in the early solar system and find that the planetary rotation is limited by impact angular momentum drain. We conclude that, assuming efficient merger of moonlets, a multiple impact scenario can account for the formation of the Earth-Moon system with its present properties.

The Moon’s origin remains enigmatic. The leading theory for the Moon’s formation posits a scenario in which a Mars-sized planetesimal impacts the late-stage accreting Earth. The ejected material produces an Earth-orbiting disk, which later gravitationally accretes to a single Moon. Impact simulations found that the projectile contributes more than 70% to the disk’s mass[1]. This skewed mass contribution is a well recognized problem as more high-precision measurements of isotopes indicate that the Moon and Earth are isotopically similar in oxygen ($^{17}\text{O}/^{16}\text{O}$ and $^{18}\text{O}/^{16}\text{O}$ within 12 ± 3 ppm[2]), titanium ($^{50}\text{Ti}/^{47}\text{Ti}$ within ± 4 ppm[3]) and pre-late veneer tungsten ($^{182}\text{W}/^{184}\text{W}$ [4]). Isotopic equilibration with a hot

protoplanetary atmosphere is efficient for oxygen but insufficient to explain the similarity in more refractory elements such as titanium[5, 3].

Deriving more disk material from the proto-Earth occurs in impact scenarios with increased angular momentum[6, 7] beyond the present value, that is later dissipated by an orbital resonance or an associated limit cycle[8]. Studies of planetary accretion[9, 10] have shown that the equal sized impactors are extremely rare unless assuming a very early event, which is inconsistent with the recent Moon formation timing estimates[11]. The expected impacts include Moon to Mars-sized impactors, supporting the specific suggested scenario of a fast spinning Earth[7], however the predicted velocity and impact parameters phase space is much wider than the preferred range (fast and low angle impactors). Alternatively, N-body simulations have been used to argue that Earth-impactors are likely to be compositionally similar to Earth, relative to other bodies[12].

In this paper, we consider a multi-impact hypothesis for Moon’s formation[13, 14]. In this scenario, the proto-Earth experiences a sequence of collisions by medium to large size bodies ($0.01 - 0.1M_{\oplus}$) (Fig. 1-a, d). Small satellites form from the impact-generated disks (1-b, e) and migrate outward controlled by tidal interactions, faster at first, and slower as the body retreats away from the proto-Earth (1-c). The slowing migration causes the satellites to enter their mutual Hill radii and eventually coalesce to form the final Moon[15] (1-f). In this fashion, the Moon forms as a consequence of a variety of multiple impacts in contrast to a more precisely tuned single impact. A similar scenario using smaller ($0.001 - 0.01M_{\oplus}$), high velocity, late accreting impactors was previously suggested[14], but supporting calculations were not provided.

N-body simulations of terrestrial planet accretion[16] show that the final angular mo-

mentum of the Earth’s system is a result of several impacts. The largest impactor is not necessary the last one. That study shows that majority of single collisions with Earth cannot form the present Moon because the impact angular momentum is insufficient relative to that of the current value, L_{EM} . Similar to the angular momentum of the Earth-Moon system, we argue that the Moon’s mass is also the result of contributions from several last impactors.

In the multi-impact scenario, the ‘compositional crisis’ described above is mitigated by two effects. First, since the mass and angular momentum of the present Earth-Moon system provide constraints on the sum of multiple impacts, rather than a single impact, the additional freedom in impact geometries enables mining more material from Earth than in the conventional scenario. Second, the oxygen signature distribution of the cumulative sum of multiple moonlets will have a reduced variance, increasing the probability of the Earth-Moon similarity compared to that from a single event.

We investigate the formation of moons by multiple impacts, and consider if Earth’s Moon specifically may have been constructed by such a mechanism. Because the Moon in this scenario is constructed in parts, we can sample a large phase space of initial conditions. We choose parameters for the impactor mass ratio γ , speed V_{imp} , direction angle β (relative to the line connecting the centers at contact), and planetary rotation ω (see Supplementary Table 1 for exact values), which resemble the characteristics of the last impactors onto Earth[16]. High velocity impactors are more frequent for smaller planetesimals because their eccentricities and inclinations are strongly affected by scattering events and distant interactions. In comparison with the classic impact scenario[1], we consider smaller masses and a larger range of angles (from head-on to near grazing impacts). In comparison with

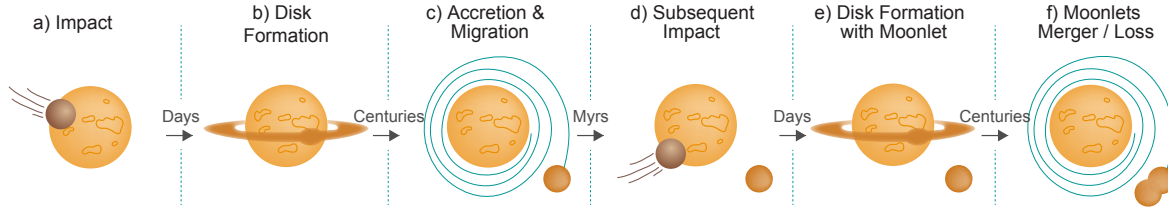


Figure 1: **Lunar formation in the multiple impact scenario.** Moon to Mars sized bodies impact the proto-Earth (a) forming a debris disk (b). Due to tidal interaction, accreted moonlets migrate outward (c). Moonlets reach distant orbits before the next collision (d), and the subsequent debris disk generation (e). As the moonlet-proto-Earth distance grows, the tidal acceleration slows, moonlets enter their mutual Hill radii. The moonlet interactions can eventually lead to moonlet loss or merger (f). The time scale between these stages is estimated from previous works [1, 17, 18].

the preferred scenario in the fast spinning Earth scenario[7], we include higher impact velocities and more slowly rotating planets.

Debris Disk

The mass of the impact-generated debris disks is evaluated relative to the present Moon’s. Of the 864 simulations performed, 750 simulations result in a disk with a discernible mass at our resolution ($> 10^{-3}M_{\text{moon}}$). The most massive disk found is $1.20M_{\text{moon}}$, which results from a graze-and-merge impact with the highest mass impactor at a speed of $\sim 1V_{\text{esc}}$, onto the most rapidly rotating target ($\omega = 0.5\omega_{\text{max}}$, where ω_{max} is the planetary rotation rate at tidal break-up) within our parameter space.

An off-axis energetic impact onto a rotating target is found to produce a debris disk

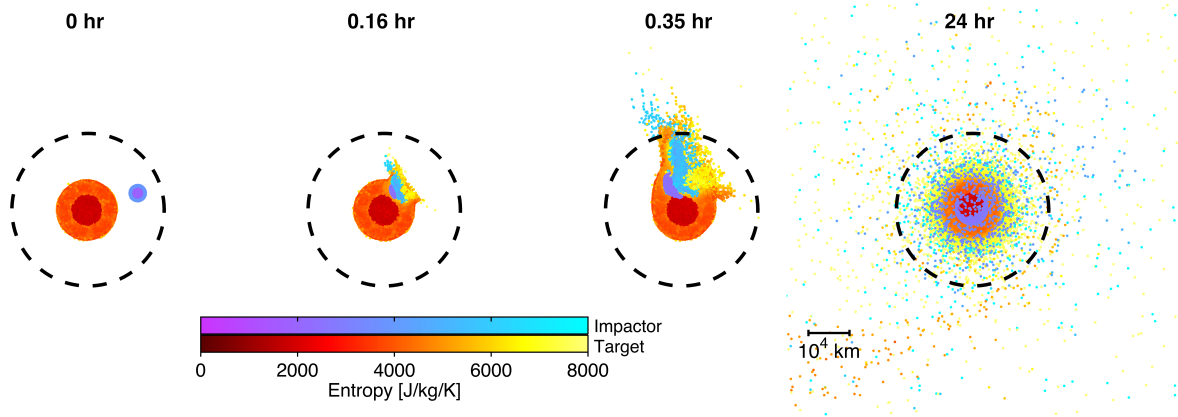


Figure 2: **Impact simulation.** Several snapshots of one of the simulation with initial conditions of $\gamma = 0.025$, $V_{\text{imp}} = 2V_{\text{esc}}$, $\beta = 30^\circ$ and $\omega = 0.5 \omega_{\text{max}}$. The color bars represent the entropy of the impactor and target. All projections are on the equatorial plane with one hemisphere removed. The impactor core is shown over the target. The Roche limit is represented by the dashed line.

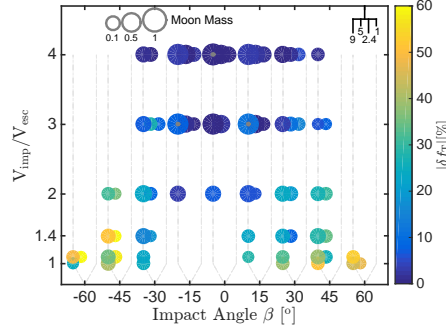
that is sourced from both impactor and target material. The cores are seen to merge, and the heating is concentrated in the upper planetary mantle (Fig. 2). The high angle impacts ($\beta = 45^\circ$) almost always produce a disk because the angular momentum of the impactor, even for relatively low velocities near V_{esc} , is sufficient to impart enough angular momentum to the ejecta to form a disk (Fig. 3). The head-on and low-angle impacts require a high velocity to eject material to orbit. Moreover, high-angle (grazing) impacts result in little mixing between the planet and the disk with the impactor contributing a substantial fraction to the disk. Low-angle impacts produce disks with higher degree of compositional similarity to Earth.

We find the composition of the disk does not strongly depend upon the retrograde sense ($L_{\text{imp}} < 0$, where the impactor’s angular momentum is opposite to that of the planet) or prograde sense ($L_{\text{imp}} > 0$) of the impact.

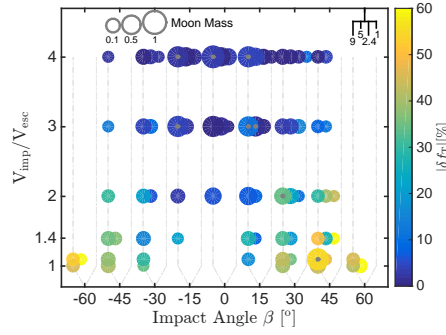
Several trends in disk mass emerge. The majority of initial conditions within the wide phase space we tested result in disks that yield a high compositional difference, $|\delta f_{\text{T}}| > 10\%$. However, the fast impactors produce disks with a low value of δf_{T} and a lack of iron. Significant fractions of the mass of fast, high angle impactors escape the system, leaving material originating from the planet’s mantle in orbit.

In addition to these trends, we also find abrupt transitions in disk mass. At high impact angles and low velocities, disk masses span a wide range varying by as much as a factor of ten. These scenarios transition from graze-and-merge to partial-accretion (previously defined[19]) as the mass ratio increases. The graze-and-merge scenario exhibits a qualitatively different character, as the impactor collides with the target a second time resulting in significantly enhanced mass ejection.

a)



b)



c)

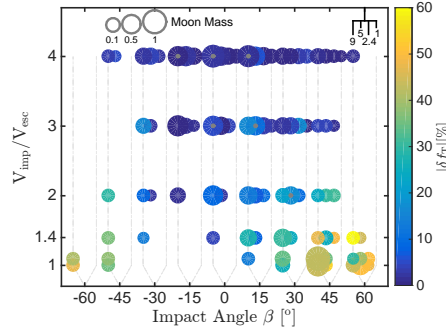


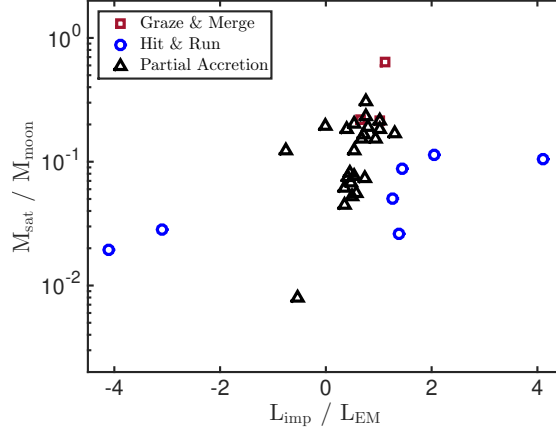
Figure 3: **Disk properties in the angle-velocity phase space.** Initial planetary rotation rate a) $\omega = 0.10\omega_{\max}$, b) $\omega = 0.25\omega_{\max}$, and c) $\omega = 0.50\omega_{\max}$. The marker size corresponds to disk mass and the color to the compositional difference between the silicates in the final planet and disk. For comparison, the grey circles in the upper left corner represent a disk mass of 0.1, 0.5 and 1 M_{Moon} . Markers are shifted horizontally according to the mass ratio, from left to right [9, 5, 2.4, 1%]. The grey dot indicates disks that have an iron content larger than the estimated lunar core mass of $0.1M_{\text{moon}}$. Disks containing < 100 SPH particles were omitted.

The mass of the satellite increases with impact angular momentum in the partial-accretion regime (Fig. 4-a). Again, the maximum satellite mass is achieved by impacts that graze-and-merge. Satellites formed by hit and run collision show large relative mass variations but they are all smaller than $\sim 0.2 M_{\text{Moon}}$.

For head-on impacts only planets with initial rotation produce a moonlet because the angular momentum required for the disk to remain stable against collapse must originate from the planetary rotation (Fig. 4-b). Head-on impacts with slow rotation produce disks with low contribution of material from the impactor. However, they lack angular momentum and a moonlet cannot form. Adding rotation to the planet increases the angular momentum of the disks, rendering the initial rotation of the planet crucial in producing moonlets by low angle impacts. The energetic hit-and-run regimes are easily distinguishable as the final angular momentum is close to the initial angular momentum (represented by the dashed lines), independent on the impactor’s angular momentum. In contrast, in the accretionary scenarios the angular momentum changes by an amount proportional to the impactor’s initial angular momentum. The resulting systems sometimes exceed L_{EM} although the values are lower than those found in past work[7, 6] because the impacts here are somewhat smaller. We note that subsequent impacts in a multiple impact scenario may further alter this value. The high angular momentum and high energy cases can cross the “hot spin stability limit”[20], explaining the Moon’s enrichment in heavy potassium isotopes[21].

We conclude that medium impactors ($0.01 - 0.1 M_{\oplus}$) can produce a sub-lunar size moonlet whose composition ranges from impactor dominated to target dominated. Near head-on impactors are preferred because they efficiently incorporate planetary material in

a)



b)

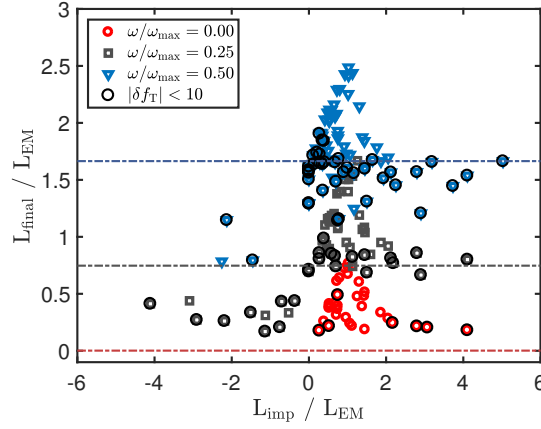


Figure 4: **Final satellite mass and system angular momentum.** a) Mass of the formed satellite using the equation (2) as a function of impact angular momentum for $\omega = 0.25 \omega_{\max}$ rotation. Colors correspond to different collisional regimes (Hit & Run - impactor escapes partially intact; Graze & Merge - impactor impacts the target twice; partial accretion - addition of mass to the target); b) The final angular momentum of all the systems which created a satellite. The different style of markers represent different initial rotations. The darker horizontal lines represent the initial planetary angular momentum value with colors corresponding to the colors of the markers. Disks containing $< 100 N_{\text{SPH}}$ were omitted.

the disk. Within the parameter space investigated, we find that the retrograde impactors often fail to form a disk with enough angular momentum to accrete a moonlet.

Proto-Earth

Post impact the planet may gain or lose mass depending on the balance of impactor merger and net erosion of material. Overall, the majority of the cases examined produce a partial or perfect merger; high energy cases result in net erosion of the planet (Supplementary Fig. 3). Extreme cases ($\gamma = 0.091$; $V_{\text{imp}} = 4V_{\text{esc}}$; $\beta = 0^\circ$ at all initial rotations) even strip half the planet’s mass. These findings are in good agreement with past studies[19], which found that planetary erosion is more common at lower impact angles than at high angles due to the larger interacting mass and interacting energy (defined in the Methods section).

For initially slowly rotating targets, the spin accelerates (the period decreases) due to typical prograde impacts (Fig. 5). However the rotation rate saturates for more rapidly rotating planets, which are difficult to accelerate further due to angular momentum drain carried away by ejected material. The retrograde impacts consistently decelerate the planet. The planetary angular momentum may be decreased by both material ejection and retrograde impacts. Hence, in the limit of a large number of impacts, angular momentum drain limits the otherwise random-walk growth of the angular momentum vector. As shown, for an initial rotation rate of 5.9 hours ($\omega = 0.25 \omega_{\text{max}}$), retrograde collisions decelerate the planet while prograde collisions hardly change the period, so that accelerating beyond this period is difficult.

Moreover, changes in the direction of the planetary spin in one single event is seldom

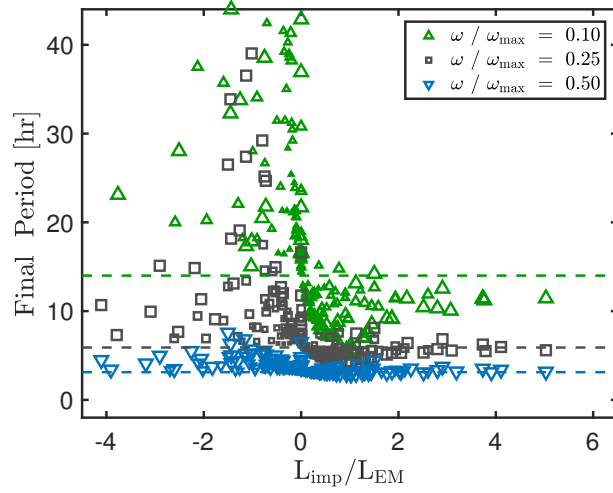


Figure 5: **Planetary rotation.** Post impact rotation as a function of the initial impact angular momentum. Marker size represents the mass of the impactor and marker style and color represent the initial rotation rate of the target, also indicated by the dashed lines for each group.

large. We observed 3 retrograde cases where the small planetary spin ($\omega = 0.1 \omega_{\text{max}}$) changed its direction. Therefore we conclude that usually subsequent moonlets will have the same sense of rotation (both prograde or both retrograde).

Disk Structure

The disk structure, including its entropy, density and vapor fraction are important in determining the constituents and efficiency of moonlet accretion. Tidal forces within the Roche limit prevent accretion, therefore the inner disk material must spread beyond the Roche limit before it can aggregate. The accretion of material outside the Roche limit is efficient, whereas the accretion of the inner disk is self-limiting because the newly spawned

moonlets at the boundary will confine the disk and cause disk mass to fall onto Earth[22]. In the accretionary simulations here disks of non-negligible mass are well extended beyond the Roche limit, with more than 60% of their mass outside this radius. Although initial rotation has been shown to somewhat reduce this fraction[23], we conclude here that the radial mass distribution of the disk is amenable to moonlet formation, subject to angular momentum constraints (discussed above).

The surface density is maximum inside the Roche limit, but is lower than in previously proposed scenarios ([6, 7, 1] as calculated by[23]) due to the lower disk mass in our scenario (Fig. 6-a,c). The initial entropy of the the disk will determine the amount of volatiles incorporated in the disk and the cooling time required to condense the silicate atmosphere[5]. We find the specific entropy is approximately constant throughout the disk, with deviations of only $\sim 10\%$ from the mean (Fig. 6-b-d). The mean entropy grows with impact energy, but while the impact energy ranges over more than two orders of magnitude, the mean entropy increases by only a factor of three. This may be understood by recognizing that the shock wave which accelerates material to bound orbits, is also responsible for heating the material. Thus the addition of kinetic and thermal energies are linked and ejected material which remains bound in the disk cannot be heated arbitrarily. When significant erosion occurs, the disk entropy is reduced because more energy is expended in ejecting material to escaping trajectories.

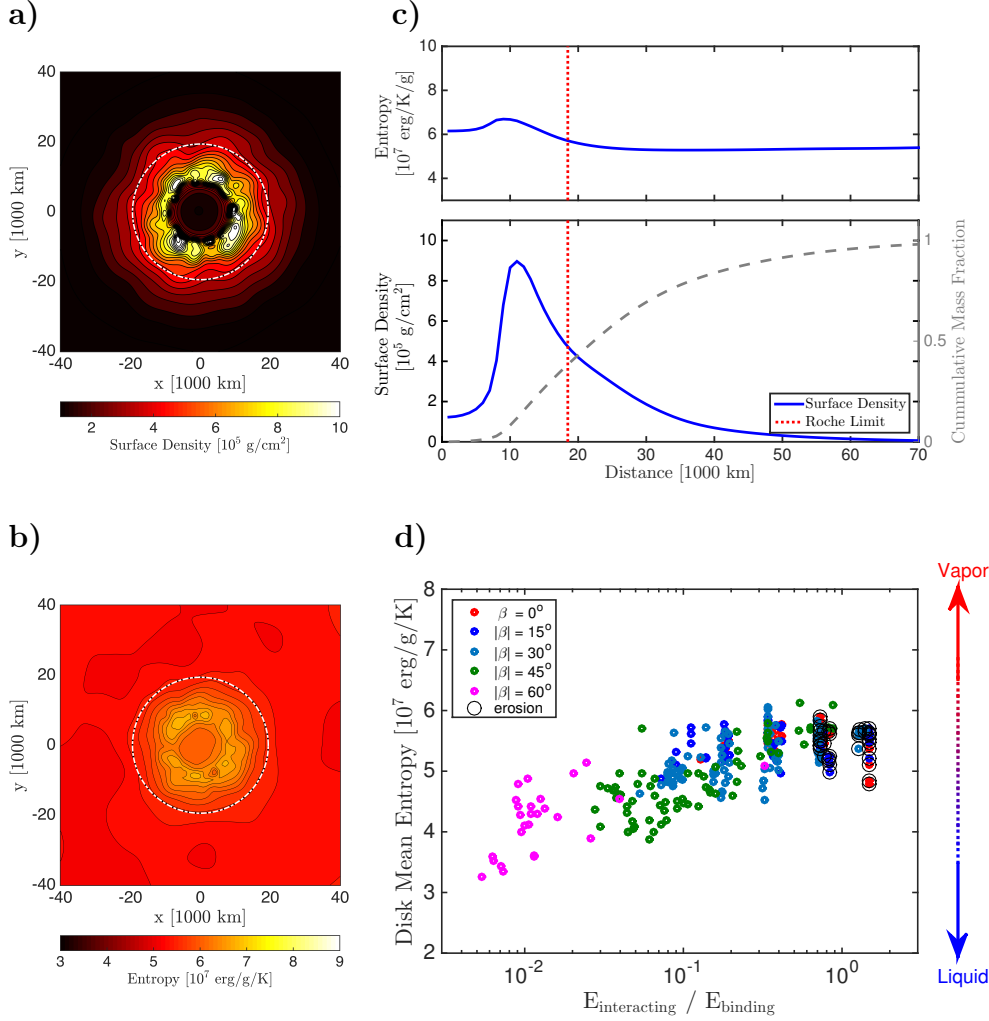


Figure 6: Disk structure post impact. 2D structure of the a) surface density b) entropy of the disk; c) Zonal average of surface density and entropy after circularization of the disk vs. the distance from the planet. The dashed lines in a-c) represent the Roche limit. The initial conditions are the same as in Fig. 2. d) For our complete set of simulations, mean entropy depends upon the energy of the interacting mass (see Methods), normalized by the gravitational binding energy of the target ($E_{\text{binding}} = GM_{\text{target}}^2/R_{\text{target}}$). Cases exhibiting planetary erosion (defined as $M_{\text{planet}} \leq 0.85M_{\text{target}}$) are indicated by black circles.

Implications for Moon Formation

By releasing some of the constraints on the impact-generated debris disk mass and system angular momentum due to individual impacts, the multiple-impact scenario allows a significantly expanded range of parameter space compared to previous Moon formation scenarios [7, 1, 24, 6]. Freedom in impact geometry and velocity allows mining more material from Earth, and the sum of such impact-generated moonlets may naturally lead to the current values of the Earth-Moon system. Most terrestrial rocks have similar ratios of $^{182}\text{W}/^{184}\text{W}$, however excess in these ratios was found for Kostomuksha komatiites rocks dated at 2.8 billion year ago [25], suggesting an unmixed mantle reservoir. Evidence of an unmixed mantle was also observed in noble gas samples [26]. Efficient mantle mixing is predicted for the single impact high angular momentum scenarios [27] erasing any primordial heterogeneity that predated Moon formation. Multiple smaller impacts promote preservation of primordial heterogeneity of Earth’s mantle, and potentially, also contribute to that of the Moon [28, 15].

We find that debris disks resulting from medium to large size impactors ($0.01 - 0.1 M_{\oplus}$) have sufficient angular momentum and mass to accrete a sub-lunar-size moonlet. We performed 1000 Monte Carlo simulations of sequences of $N = 10, 20$ and 30 impacts each, in order to estimate the ability of multiple impacts to produce a Moon-like satellite. The impact parameters were drawn from distributions previously found in terrestrial formation dynamical studies [18]. With perfect accretionary mergers, approximately half the simulations result in a moon mass that grows to its present value after ~ 20 impacts (see Supplementary Material). We verified that the standard deviation of the $\Delta^{17}\text{O}$ difference between the growing moon and target is reduced initially as \sqrt{N} , as expected.

After ~ 20 impacts (roughly equivalent to the target mass) the compositional difference stabilizes, with each growing body maintaining a signature, owing to different proportions contributed by the incoming sources. In the canonical giant impact scenario, only $\sim 1-2\%$ of impactors lead to the observed compositional similarity (assuming the same impactor composition distribution as described, and that the impactor constitutes $60-80\%$ of the disk[29, 30]), while in multiple impact scenarios the fractions of successful simulations increases to 10's %, with the precise values depending on the assumed distribution. The range of conditions producing a Moon-mass satellite with terrestrial composition is confined to narrow set of conditions of fast ($V/V_{\text{esc}} \sim 4$), near head-on events ($\beta \sim 0$). If multiple impacts are considered, additional components with lower impact velocity are allowed, such as $V/V_{\text{esc}} \sim 2$ with $|\beta| < 30^\circ$. This occurs to some extent because of the reduction of the variance composition in averaging multiple components, but also importantly, because there are regions in phase space where the predicted moonlet masses are small and the compositions are Earth-like. Such sub-lunar components can still provide the building blocks for the final Moon, while in the single impact hypothesis they are rejected due to their small mass.

Preimpact planetary rotation promotes moonlet formation by facilitating the formation of a more massive disk from more loosely bound planetary material, and by increasing the angular momentum of the disk, stabilizing it against collapse. But the preimpact rotation rate is limited. Our hydrodynamic simulations show that multiple impactors with isotropic directions cannot accelerate the planet to breakup rotation due to angular momentum drain by escaping material. The rotation of an Earth-like target begins to saturate at a period ~ 5.9 hours, in contrast to previous calculations[16] which assume

perfect merger. Faster rotation rates may be conceivably achieved by rare single large events, but they are not expected to develop from the sum of multiple collisions. This is validated by the Monte Carlo simulations of impact sequences showing the vast majority of cases remain within the range $-0.5\omega_{\max} \leq \omega \leq 0.5\omega_{\max}$ (Supplementary Fig. 4-c). For sequences of 10, 20, and 30 impacts, the planetary spin migrated outside this range for only 1, 7, and 13% of the cases, respectively. Most cases have a final rotation rate $-0.2\omega_{\max} \leq \omega \leq 0.2\omega_{\max}$. This neglects the change in planetary rotation due to moonlet tidal evolution, that would generally decrease the spin rate.

The preferred scenario of the single-impact high angular momentum case[7] invokes a small retrograde impactor that produces a massive satellite due to the rapid initial rotation assumed for the planet (near the breakup rate). Our conclusions, on the limited planetary rotation gain and the resulting debris disk masses, point to typical individual moonlet masses being considerably below the present Moon mass. Specific scenarios that exceed one lunar mass may be constructed. However, the broad range we find within the typical parameter space that leads to sub-lunar mass disks, supports the notion that the Earth’s Moon was formed by the merger of multiple moonlets.

Satellite pairs formed by the same impact were found to be mostly unstable[31], leading to moonlet-Earth collisions, moonlet-moonlet mergers or scattering. High percentage of moonlet merger was found for cases in which the inner moonlet is larger, hence tidally evolves faster than the outer moonlet. The multiple impact scenario operates on longer timescales, allowing even a smaller inner moonlet to reach the Hill Radius of the outer moonlet in suitable time (~ 100 Myr for a $0.1 M_{\text{moon}}$ inner moonlet and a $0.9 M_{\text{moon}}$ outer moonlet at $30 R_{\text{Earth}}$, assuming current tidal values). Moreover, the survival of an

accreted moonlet depends also on the planetary environment, as collisionless encounters of leftover planetesimals can excite the satellite’s eccentricity and possible loss[32]. Future work will address the new dynamics and merger efficiency of the accreted moonlets to a final Moon.

Methods

We probe a broad phase space by simulating impact scenarios with ranging values of the impactor’s velocity, mass, angle, and initial rotation of the target. We use Smoothed Particle Hydrodynamics (SPH) to simulate impacts in the gravity dominated regime, using the astrophysical code Gadget2[33]. In this implementation, the individual evolution of spherically symmetric particles is tracked in 3 dimensions. The spatial distribution of each particle is defined by a spline density weighting function, known as the kernel, and a characteristic radius, known as the smoothing length. The functional form of the kernel does not change during the simulation, but the smoothing length of each particle is varied in order to maintain a constant desired number of overlapping particles, or neighbors. This procedure allows low-density regions to be resolved, although spatial resolution is reduced. The kinematic state of each particle is evolved due to gravity, compressional heating/expansional cooling, and shock dissipation. Material strength and fracture are neglected, and for the simulated time of the impact (\sim a day) radiative processes may be ignored. A standard prescription of artificial viscosity is used in order to mimic shock dissipation.

We employ a tabulated equation of state which was generated using the well-tested

semi-analytical equation of state M-ANEOS[34] with forsterite comprising the mantle and iron comprising the core.

We performed over 800 simulations consisting of 10^5 SPH particles to span the parameter space and a smaller number of high resolution simulations with 10^6 particles to better define the characteristics of the disk.

For ease of comparison with previous work[7, 29], all impacts are assumed to occur in the equatorial plane of the target. The runs cover 24 hours of simulation time after impact. In order to test consistency of our hydrodynamic code and analysis algorithms, we reproduced previously published scenarios[7] and obtained small differences (*e.g.*, $< 5\%$ in disk mass).

We use a target with a mass of ~ 1 Earth mass because we assume that the Moon-forming impacts occur near the final stages of the planet’s accretion when the target mass changes by a relatively small amount with each impact. In off-axis impacts, the fraction of the impactor mass whose projected initial trajectory intersects the planet is referred to as the interacting mass, $M_{\text{interacting}}$, with kinetic energy $E_{\text{interacting}}$.

We validated our assumption that previous accreted moonlets do not change the initial outcome of the disk, by simulating impacts on targets with an orbiting moon. We chose a Mars-sized orbiting body with a range of semimajor axes, from the closest stable orbit in the SPH simulation to the current location of the Moon $((1.2 - 20)R_{\text{Roche}})$ and an equal sized impactor. The results show that a pre-existing moonlet does not affect the disk (mass and composition) as long as it is not close to the Roche limit $(> 3 R_{\text{Roche}})$. For very close-in satellites, the impact can induce collision in the planet-moon system. For very distant satellites, the impact can excite the moons into escaping trajectories.

Massive moons, like the one tested, will migrate quickly after their formation due to tidal dissipation ($\sim O(3)$ yr from R_{Roche} to $3 R_{\text{Roche}}$ for current dissipation parameters), hence preexisting moons will be distant enough before the next impactor so that we may restrict our attention to simulating only two bodies. We note that, we test only the first ~ 24 hours after the impact, while the longer disk evolution can be affected by resonances and angular momentum transfer with pre-existing moons[35].

Impact Characteristics

We characterize the impact event by determining the mass of the disk produced, mass of the planet and angular momentum and composition of the components. After each simulation we follow an iterative procedure[6, 36] to classify particles into one of three categories: planet particles whose angular momentum is insufficient to escape the gravitational pull of the planet; disk particles whose orbital pericenter is outside the planetary radius, and escaping particles, which are gravitationally unbound. We chose to classify disk particles as those with periapsis distance larger than the equatorial radius of the planet, as opposed to using the semimajor axis equivalent distance ($a_{\text{eq}} = l_z^2 / GM_{\text{planet}}$), because the latter overestimates the disk mass in cases where the disk particles are not vaporized, eccentric, and not likely to further gravitationally interact. (We note that in high energy and high angular momentum cases[20], this distinction is irrelevant). In this classification we neglect pressure gradients as particles are assumed to travel on Keplerian orbit, as would solid particles.

The compositional difference between the silicates in the final planet and disk is defined as[6, 7]:

$$\delta f_{\text{T}} = [f_{\text{disk,tar}}/f_{\text{planet,tar}} - 1] \times 100, \quad (1)$$

where $f_{\text{disk,tar}}$ and $f_{\text{planet,tar}}$ are the mass fractions of silicate originating from the target in the disk and the final planet, respectively. A value of $\delta f_{\text{T}} < 0$ implies that the disk contains more material derived from the impactor than from the target. If the impactors had the same isotopic composition as Mars then the compositional constraint allows only $|\delta f_{\text{T}}| < 2$ [5], however the projectile may have been more similar to Earth than to Mars [12]. The sum of multiple disks will contribute to the final moon's composition, so each disk can vary to some extent while maintaining an average of small $|\delta f_{\text{T}}|$.

The slower accretion of the moonlet from the disk is not simulated but estimated from the calculated disk mass, M_{disk} , and its angular momentum, L_{disk} , using results from previous N-Body simulations [17]:

$$M_{\text{sat}} = 1.9 \cdot \frac{L_{\text{disk}}}{\sqrt{GM_{\text{planet}}a_{\text{R}}}} - 1.15M_{\text{disk}} - 1.9M_{\text{esc}}, \quad (2)$$

where G is the gravitational constant. This relation is an estimate for the satellite mass as the exact accretion efficiency is still uncertain. We assume that the escaped mass during the accretion process is negligible ($M_{\text{esc}} = 0$) as in previous studies [6, 7]. The equation is not valid for disks with high specific angular momentum (yielding $M_{\text{sat}} > M_{\text{disk}}$) that correspond to a moon accretion at distances greater than $1.3 R_{\text{Roche}}$. We neglect the disks that yield a negative angular momentum compared with Earth, as a moonlet in a retrograde orbit will experience tidal acceleration that will lower the semimajor axis until it collides with the planet.

We assume that initially eccentric and inclined disks are circularized and flattened as collisions between particles in the disk will lead in a few orbital periods to decrease in orbital eccentricities and inclinations while angular momentum is conserved. The final semimajor axis of each disk particle is $a_{\text{eq}} = l_z^2 / GM_{\text{planet}}$, where l_z is the specific angular momentum of the particle normal to the equatorial plane of the planet. By lowering all the disk particles to the equatorial plane, assigning them a random phase and smoothing them according to the kernel function, we calculate the surface density and specific entropy of the disk at any given point.

Monte Carlo Simulations

We performed Monte Carlo simulations of impact sequences by drawing impacts parameters (mass ratio, $V_{\text{imp}}/V_{\text{esc}}$, impact angle β) within our phase space of interest and distributions based on previous terrestrial formation studies [18]. The angle distribution is symmetric, allowing retrograde and prograde impacts. Due to the uncertainty in the impact parameters, we also separately examined sequences of high velocities ($2.5 - 4V_{\text{esc}}$) and low velocities ($1 - 2.5V_{\text{esc}}$) impactors. The impactor mass ratio of interest in this work is 1-9%, the upper limit corresponding to the approximate isolation mass[37] (the protoplanetary mass expected to accrete by the oligarchic growth in the early planetesimal disk) of the inner solar system. Although rare larger events are possible, our goal here is to demonstrate the feasibility of a scenario consisting of multiple smaller events. Each impactor has a distinct compositional signature drawn from a normal distribution with a standard deviation of a Mars-like composition[5].

For every simulated impact, we perform a linear interpolation within our phase space

to determine post impact conditions such as planetary rotation spin, moonlet mass, iron disk content and the impactor contribution to the disk and planet. The planetary spin and signature is evolved from one impact to the next. The final Moon’s characteristics are calculated assuming perfect moonlet accretion and the difference between the planet’s silicate composition and that of the growing moon’s is tested. By assuming that the iron fraction in the disk is preserved in the accreted moonlet, we estimate the iron fraction in the final moon. The final angular momentum of the system is obtained from the sum of the individual disk angular momenta with Earth’s final value. Perfect accretion of moonlets is assumed as a simplification, as the details and probabilities of various multi moonlet evolutionary paths are yet unknown.

Code availability

The code used to generate the hydrodynamic simulations can be accessed <https://www.mpa-garching.mpg.de/gadget/>.

Data availability

The data that support the findings of this study are available from the corresponding author upon request.

References

- [1] Canup, R. M. Simulations of a late lunar-forming impact. *Icarus* **168**, 433–456 (2004).
- [2] Herwartz, D., Pack, A., Friedrichs, B. & Bischoff, A. Identification of the giant impactor Theia in lunar rocks. *Science* **344**, 1146–1150 (2014).
- [3] Zhang, J., Dauphas, N., Davis, A. M., Leya, I. & Fedkin, A. The proto-earth as a significant source of lunar material. *Nature Geoscience* **5**, 251–255 (2012).
- [4] Kruijer, T. S., Kleine, T., Fischer-Godde, M. & Sprung, P. Lunar tungsten isotopic evidence for the late veneer. *Nature* **520**, 534–537 (2015).
- [5] Pahlevan, K. & Stevenson, D. J. Equilibration in the aftermath of the lunar-forming giant impact. *Earth and Planetary Science Letters* **262**, 438–449 (2007).
- [6] Canup, R. M. Forming a moon with an earth-like composition via a giant impact. *Science* **338**, 1052–1055 (2012).
- [7] Ćuk, M. & Stewart, S. T. Making the moon from a fast-spinning earth: A giant impact followed by resonant despinning. *Science* **338**, 1047–1052 (2012).
- [8] Wisdom, J. & Tian, Z. Early evolution of the earth-moon system with a fast-spinning earth. *Icarus* **256**, 138 – 146 (2015).
- [9] Jacobson, S. A. & Morbidelli, A. Lunar and terrestrial planet formation in the grand tack scenario. *Philosophical Transactions of the Royal Society of London A: Mathematical, Physical and Engineering Sciences* **372** (2014).

- [10] Kaib, N. A. & Cowan, N. B. The feeding zones of terrestrial planets and insights into moon formation. *Icarus* **252**, 161 – 174 (2015).
- [11] Jacobson, S. A. *et al.* Highly siderophile elements in earth/'s mantle as a clock for the moon-forming impact. *Nature* **508**, 84–87 (2014).
- [12] Mastrobuono-Battisti, A., Perets, H. B. & Raymond, S. N. A primordial origin for the compositional similarity between the earth and the moon. *Nature* **520**, 212–215 (2015).
- [13] Citron, R., O.Aharonson & Peretz, H. Moon formation from multiple impact events. *LPSC* **2085** (2014).
- [14] Ringwood, A. Flaws in the giant impact hypothesis of lunar origin. *Earth and Planetary Science Letters* **95**, 208 – 214 (1989).
- [15] Jutzi, M. & Asphaug, E. Forming the lunar farside highlands by accretion of a companion moon. *Nature* **476**, 69–72 (2011).
- [16] Agnor, C. B., Canup, R. M. & Levison, H. F. On the character and consequences of large impacts in the late stage of terrestrial planet formation. *Icarus* **142**, 219 – 237 (1999).
- [17] Ida, S., Canup, R. M. & Stewart, G. R. Lunar accretion from an impact-generated disk. *Nature* **389**, 353–357 (1997).
- [18] Raymond, S. N., O'Brien, D. P., Morbidelli, A. & Kaib, N. A. Building the terrestrial planets: Constrained accretion in the inner solar system. *Icarus* **203**, 644 – 662 (2009).

- [19] Stewart, S. T. & Leinhardt, Z. M. Collisions between gravity-dominated bodies.
ii. the diversity of impact outcomes during the end stage of planet formation. *The Astrophysical Journal* **751**, 32 (2012).
- [20] Lock, S. J. & Stewart, S. T. A hot spin stability limit for terrestrial planets. *LPSC* **2856** (2016).
- [21] Wang, K. & Jacobsen, S. B. Potassium isotopic evidence for a high-energy giant impact origin of the moon. *Nature advance online publication*, – (2016).
- [22] Salmon, J. & Canup, R. M. Accretion of the moon from non-canonical discs. *Philosophical Transactions of the Royal Society of London A: Mathematical, Physical and Engineering Sciences* **372** (2014).
- [23] Nakajima, M. & Stevenson, D. J. Investigation of the initial state of the moon-forming disk: Bridging SPH simulations and hydrostatic models. *Icarus* **233**, 259 – 267 (2014).
- [24] Reufer, A., Meier, M. M., Benz, W. & Wieler, R. A hit-and-run giant impact scenario. *Icarus* **221**, 296 – 299 (2012).
- [25] Touboul, M., Puchtel, I. S. & Walker, R. J. 182W evidence for long-term preservation of early mantle differentiation products. *Science* **335**, 1065–1069 (2012).
- [26] Mukhopadhyay, S. Early differentiation and volatile accretion recorded in deep-mantle neon and xenon. *Nature* **486**, 101–104 (2012).

- [27] Nakajima, M. & Stevenson, D. J. Melting and mixing states of the earth’s mantle after the moon-forming impact. *Earth and Planetary Science Letters* **427**, 286 – 295 (2015).
- [28] Robinson, K. L. *et al.* Water in evolved lunar rocks: Evidence for multiple reservoirs. *Geochimica et Cosmochimica Acta* **188**, 244 – 260 (2016).
- [29] Canup, R. M. Lunar-forming collisions with pre-impact rotation. *Icarus* **196**, 518 – 538 (2008). Mars Polar Science IV.
- [30] Canup, R. M. Dynamics of lunar formation. *Annual Review of Astronomy and Astrophysics* **42**, 441–475 (2004).
- [31] Canup, R. M., Levison, H. F. & Stewart, G. R. Evolution of a terrestrial multiple-moon system. *The Astronomical Journal* **117**, 603 (1999).
- [32] Pahlevan, K. & Morbidelli, A. Collisionless encounters and the origin of the lunar inclination. *Nature* **527**, 492–494 (2015).
- [33] Springel, V. The cosmological simulation code gadget-2. *Monthly Notices of the Royal Astronomical Society* **364**, 1105–1134 (2005).
- [34] Melosh, H. A hydrocode equation of state for SiO₂. *Meteoritics & Planetary Science* **42**, 2079–2098 (2007).
- [35] Charnoz, S., Salmon, J. & Crida, A. The recent formation of saturn’s moonlets from viscous spreading of the main rings. *Nature* **465**, 752–4 (2010).

- [36] Canup, R. M., Ward, W. R. & Cameron, A. A scaling relationship for satellite-forming impacts. *Icarus* **150**, 288–296 (2001).
- [37] Kokubo, E., Kominami, J. & Ida, S. Formation of terrestrial planets from protoplanets. i. statistics of basic dynamical properties. *The Astrophysical Journal* **642**, 1131 (2006).

Acknowledgments

We thank S. Stewart and R. Citron for providing guidance on the computational code, as well as A. Mastrobuono-Battisti for providing the data used for the Monte Carlo simulations. This project was supported by the Minerva Center for Life Under Extreme Planetary Conditions as well as by the I-CORE Program of the PBC and ISF (Center No. 1829/12). RR is grateful to the Israel Ministry of Science, Technology and Space for their Shulamit Aloni fellowship. HBP also acknowledges support from the Israel-US binational science foundation, BSF grant number 2012384, and the European union career integration grant “GRAND”.

Author Contribution

RR performed the SPH simulations and their analysis with guidance by OA. HBP suggested the multiple impact idea. All authors contributed to discussions, interpretations and writing.

Competing Financial Interest

The authors declare no competing financial interests.

Supplementary material : A Multiple Impact Origin for the Moon

Raluca Rufu^{1*}, Oded Aharonson¹, Hagai B. Perets²

¹Weizmann Institute of Science, Department of Earth and Planetary Sciences, Center for Planetary Science, Rehovot 76100, Israel

² Technion Israel Institute of Technology, Physics Department, Haifa 32000, Israel.

* Contact Information: e-mail: Raluca.Rufu@weizmann.ac.il

Contents

1	Supplemental Methods	2
1.1	Equation of State	2
1.2	Impact simulations	2
2	Supplemental Results	3
2.1	Debris Disk	3
2.2	Planetary Erosion	6
2.3	Monte Carlo Simulations	6
3	Supplemental Movie Caption	7
4	Supplemental Result Table Caption	8

Other Supplementary Material for this manuscript includes the following:
 Movie S1
 Table of Results

1 Supplemental Methods

1.1 Equation of State

We employ a tabulated equation of state which was generated using the well-tested semi-analytical equation of state M-ANEOS [1] with forsterite comprising the mantle and iron comprising the core. ANEOS uses the temperature and density as independent variables and thermodynamic quantities are derived from the Helmholtz free energy, described by the sum of the zero-temperature free energy, thermal energy of the collective motion of the nuclei, and an electronic ionization term. The equation of state describes a mixed vapor-fluid state in a single SPH particle, assuming that the phases are in temperature and pressure equilibrium, therefore the mass fraction of each state can be calculated. M-ANEOS is a revised version of ANEOS [2] which adds another 8 parameters (a total of 45 parameters) to describe diatomic molecular vapor that previously treated all vapor as monoatomic species instead of molecular gas phases (mostly SiO_2 and O_2), hence the entropy required for vaporization was overestimated. It should be noted that M-ANEOS (and ANEOS) cannot account for metastable states as perfect thermodynamic equilibrium and perfect reversibility is assumed.

1.2 Impact simulations

We performed over 500 simulations consisting of $N \sim 10^5$ SPH particles to span the parameter space and a smaller number of high resolution simulations with $N \sim 10^6$ particles to better define the characteristics of the disk. We choose parameters for the impactor mass ratio γ , speed V_{imp} , angle β , and planetary rotation ω (Supplementary Table 1).

The colliding bodies contain 30% core and 70% mantle material, similar to current Earth, and are generated with isentropic thermal profiles with a surface temperature of 2000K comparable to a 'warm start' in previous studies [3]. The objects are simulated in isolation for 24 hours to allow their initial relaxation and to establish gravitational equilibrium. Rotation is added to a stable planet and is simulated again in order to re-establish equilibrium.

We characterize the impact event by determining the mass of the resulting disk and planet, as well as the angular momentum and composition of the components. After each simulation we follow an interactive procedure [4, 5] to classify particles into one of three categories: planet particles whose angular momentum is insufficient to escape the gravitational pull of the planet; disk particles, distinguished from the planet, by their orbital periapses falling outside the planetary radius, and escaped particles, which are gravitationally unbound. In this classification we neglect pressure gradients as particles are assumed to travel on Keplerian orbit, as would be the case for non-interacting solid particles. An initial guess is made for the planet's mass, M_{planet} , and flatness, f . Assuming a terrestrial density of $\rho_{\oplus} = 5.5 \text{ g/cm}^3$, the oblate spheroid equatorial radius is:

$$R_{\text{eq}} = \left(\frac{3}{4\pi\rho_{\oplus}} M_{\text{planet}} \frac{1}{1-f} \right)^{1/3}. \quad (1)$$

An alternative to the condition comparing R_{eq} to the periapses distance is to compare it to the semimajor-axis equivalent distance ($a_{\text{eq}} = l_z^2/GM_{\text{planet}}$). Although for low eccentricity trajectories the two conditions were found to agree [5], we found that in some of the conditions they may differ by as much as a factor of three in the total disk mass. This difference plays a more significant role in less massive disks, such as the ones considered here, as the energy dissipation time scale is larger than the collision time of the particle with the planet. We therefore choose the periapses condition as it is the more rigorous threshold in our simulations. To treat particle aggregates, we search for particles outside the planetary radius with $\rho > 1 \text{ g/cm}^3$, and sort them into density 'clumps'. Each group is assigned a uniform classification according to the dynamics of its center of mass, similar to past treatments [6].

The mass and angular momentum of the ejected particles (disk+escaped) are used to calculate a new estimate for the planet's mass and its rotation (ω_{planet}). A new flatness parameter is calculated using:

$$f = \frac{5}{2} \left(\frac{\omega_{\text{planet}}}{\omega_{\text{max}}} \right)^2 / \left[1 + \left(\frac{5}{2} - \frac{15K}{4} \right)^2 \right], \quad (2)$$

where ω_{max} is the maximum rotation before break-up and K is the gyration constant (for Earth $K = 0.335$, for a uniform density sphere $K = \frac{2}{5}$). This value of f and M_{planet} is then used to calculate a new R_{eq} . The algorithm is repeated until convergence.

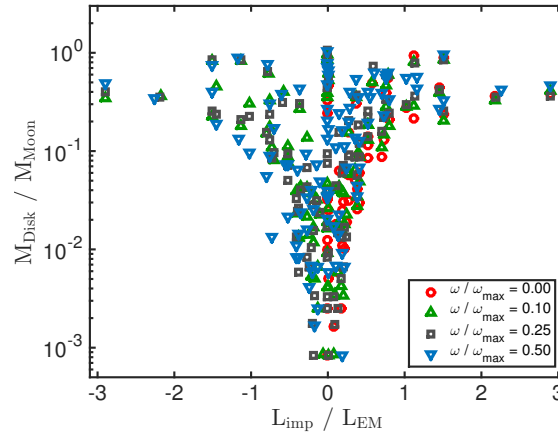
2 Supplemental Results

2.1 Debris Disk

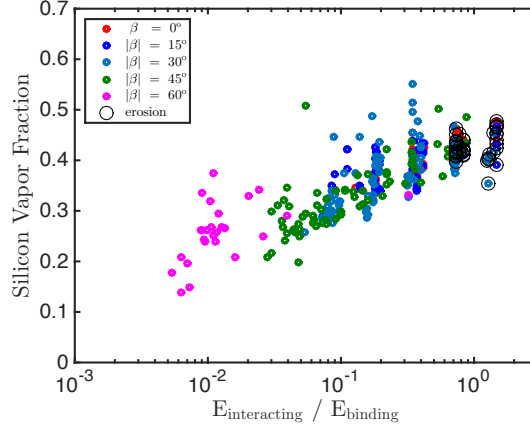
The general trend observed in the disk mass is that the non-head-on ($\beta \geq 15^\circ$) and prograde impacts ($L_{\text{imp}} > 0$, where the impactor's angular momentum is in the same direction as that due to the planetary spin) result in disks increasing in mass as a function of angular momentum, until a maximum is reached and excess angular momentum causes material to escape the system at the expense of the disk (Supplementary Figure 1). The maximum disk mass is higher with increasing rotation rate, as material is more loosely bound to the planet and is ejected from the surface more easily. For the retrograde impacts ($L_{\text{imp}} < 0$), disk mass still increases with absolute angular momentum, however peaks at a reduced value. The mass of the disk does increase for a prograde impact by a factor of 2 relative to retrograde (keeping other parameters constant), because the latter has a lower total angular momentum, and the disk is correspondingly less massive (Supplementary Figure 1).

	Parameter	Values
mass ratio	γ	0.010, 0.024, 0.053, 0.091
impact velocity	$V_{\text{imp}}/V_{\text{esc}}$	1.0, 1.1, 1.4, 2.0, 3.0, 4.0
impact angle	$\beta [^\circ]$	0, ± 15 , ± 30 , ± 45 , ± 60
planetary rotation	$\omega/\omega_{\text{max}}$	0.00, 0.10, 0.25, 0.50

Supplementary Table 1: **Values of the different initial conditions assumed.** The parameters are represented by γ , the mass ratio between the impactor and total mass, V_{imp} , the impact velocity normalized by the mutual escape velocity at contact, β , the impact angle defined as the angle between the centers of the bodies at contact and the velocity of the impactor, ω initial rotation rate of the proto-Earth normalized by ω_{max} , the maximum rotation rate before break-up.



Supplementary Figure 1: **Disk mass as a function of impact angular momentum for low impact angles ($|\beta| \leq 30^\circ$).** The different markers style represents different initial rotations.



Supplementary Figure 2: **Disk thermodynamics as a function of impact energy.** Vapor fraction as a function of the energy of the interacting mass (defined in the Methods section in the main text), normalized by the gravitational binding energy of the target ($E_{\text{binding}} = GM_{\text{target}}^2/R_{\text{target}}$). Cases exhibiting planetary erosion (defined as $M_{\text{planet}} \leq 0.85M_{\text{target}}$) are indicated by black circles.

The energetics of the disk will determine the initial thermal state of each moonlet. Because the time between impacts is short, of order Myrs, moonlets may retain much of this initial heat (and associated melt) until subsequent merger.

The silicon vapor fraction is calculated by summing the masses of the particles in a single vapor phase and the particles in the two phase state multiplied by the vapor fraction for each particle (X_{vap_i}) using the relation:

$$X_{\text{vap}_i} = \frac{S_i - S_{\text{liq}}(T_i)}{S_{\text{vap}}(T_i) - S_{\text{liq}}(T_i)}, \quad (3)$$

where S_i is the specific entropy of the SPH particle, $S_{\text{liq}}(T_i)$ and $S_{\text{vap}}(T_i)$ are the specific entropies of the liquid and vapor phase boundary, respectively, at temperature T_i of the particle i .

The silicon vapor fraction in the disk (shown in Supplementary Figure 2) ranges from $\sim 10 - 70\%$ with low angle impacts angles exhibiting the maximum value.

Previous work [7] of high-resolution Moon forming impacts using grid-based simulations, suggests that a disk composed of mainly silica vapor will not be sufficiently stable to accrete into a large Moon owing to fast angular momentum transfer associated with spiral shocks. However, the only tested scenario was similar to the canonical impact [8] and the two polytrope equations of state chosen are not able to mimic the phase changes in the mantle [6]. Future work is still needed to determine whether high vapor fraction disks are suitable for Moon forming scenarios, as well as to account for lower disk mass and preexisting moons in current accretion models [9].

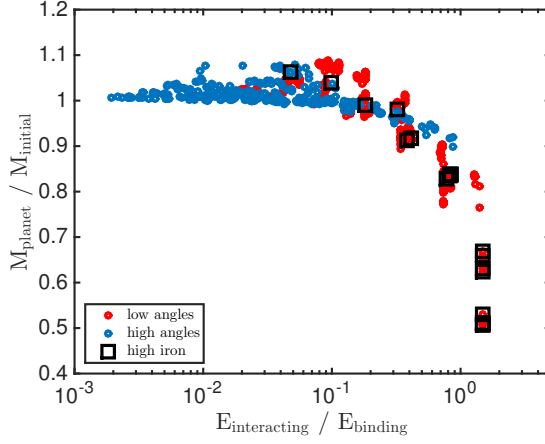


Figure 3: **Mass of the planet after impact as a function of the energy of the interacting mass.** The interacting mass is defined as the total energy of the impact scaled by the fraction $M_{\text{interacting}}/M_{\text{impactor}}$ and is normalized by the binding energy of the target ($GM_{\text{target}}^2/R_{\text{target}}$). The blue circles represent impacts with high angles ($|\beta| > 30^\circ$), the red represent the low angles ($|\beta| \leq 30^\circ$). The black squares represent disk with a larger iron content than the Moon’s core.

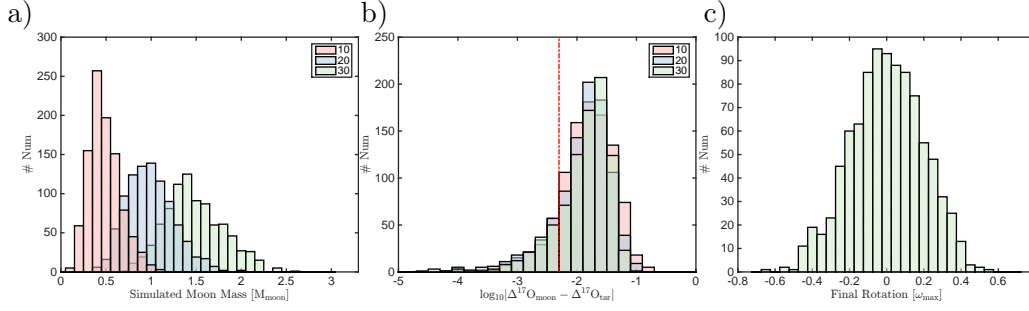
2.2 Planetary Erosion

The impact parameter space is mostly composed of partial accretion impacts. Extremely high energy impacts caused severe erosion to the planet and contaminated the disk with core target material. In these cases, the iron fraction of the disk is larger than the estimated amount in the present Moon (Supplementary Figure 3). Also, since mantle material is preferentially ejected relative to the core, the iron fraction in the target grows (up to 60%) for increasingly erosional collisions. For these cases to be relevant for Moon formation scenarios, we would need a smaller initial cores.

2.3 Monte Carlo Simulations

We perform monte Carlo simulations of impact sequences by drawing impacts parameters from our phase space (mass ratio, $V_{\text{imp}}/V_{\text{esc}}$, impact angle β) with similar distributions found in previous terrestrial formation studies [[10]. We also separately examined sequences of high velocities impactors ($2.5 - 4 V_{\text{esc}}$) and low velocities ($1 - 2.5 V_{\text{esc}}$) due to uncertainty in the distribution of impact parameters.

For a sequence of 20 impacts, the final Moon is massive enough ($\geq M_{\text{moon}}$) in 40% of the cases. 17% of simulations with sequences of 20 impacts have a signature difference small enough to reproduce the oxygen isotope signature difference in the Earth-Moon system ($\Delta^{17}\text{O} \leq 0.005\text{‰}$). For a population of high velocity impactors ($2.5 - 4 V_{\text{esc}}$), the compositional similarity increases to



Supplementary Figure 4: **Monte Carlo simulations.** Histogram of a) final moon mass; b) the compositional difference between the final moon and the target. Color bars represent different number of impact sequences. The red dashed line represents the Earth-Moon oxygen isotope upper limit difference (Young2016). c) The final rotation of the planet assuming sequence of 30 impacts.

36%. This population of impactors tends to excavate more planetary material, and additionally in some cases a large part of the impactor escapes. In contrast, for a population of low velocities impactors ($1 - 2.5 V_{\text{esc}}$), the compositional similarity is achieved in 13% of the cases. This population of impactors is often in the part of phase space where graze and merge is common, contributing more impactor material to more massive disks than in the faster regime.

The iron fraction of the final Moon was less than 10% (the estimated upper limit [5] for more than 75% (98%/60%, for high/low impactor velocity subsets) of the cases. The absolute values of the final angular momentum of the systems have a median of $0.5 L$, and $\sim 10\%$ of cases ($<1\%/17\%$ for high/low velocity subsets) have a final value exceeding L_{EM} .

The final angular momentum resulting from multiple impacts is arbitrarily set by the last few impactors. A value greater than L_{EM} , is reached throughout the evolution of a 20 impact sequence in $\sim 50\%$ of the cases, making the $1 L_{\text{EM}}$ value feasible in this scenario. Importantly, further changes to the total angular momentum are possible by dynamical processes including the evection resonance or an associated limit cycle [11], moonlet escape reducing the angular momentum, or semicollisional accretion [12] increasing the angular momentum.

3 Supplemental Movie Caption

Movie 1 : Example of formation of a sub-lunar disk. The impact uses a $\gamma = 0.025$ impactor with a velocity of $2V_{\text{esc}}$, at an impact angle of $\beta = 30^\circ$ and a fast initial planetary rotation ($0.5 \omega_{\text{max}}$). The color bars represent the entropy of the impactor and target. The movie captures the equatorial plane cross-section and the two parts overlap for display reasons. To emphasis the merging of the cores, the impactor core is shown over the target. The Roche limit is represented by the dashed line.

4 Supplemental Result Table Caption

Table 1: Impact outcomes. ω - initial spin of the target, normalized by the break-up rotation ω_{\max} . γ - impactor mass ratio $M_{\text{imp}}/M_{\text{tot}}$. V_{imp} - velocity of the impactor in cm s^{-1} . β impact angle in degrees, negative values indicate retrograde impacts as compared to the planet spin vector. $L_{\text{planet Initial}}$ the initial angular momentum of the planet [L_{EM}]. L_{imp} - impactor angular momentum [L_{EM}]. M_{disk} - mass of the disk [M_{moon}]. M_{esc} - escaped mass [M_{moon}]. M_{planet} - final planet mass [M_{\oplus}]. M_{sat} - mass of the satellite [M_{moon}]. L_{planet} - final planetary angular momentum [L_{EM}]. L_{disk} - final disk angular momentum [L_{EM}]. Iron in disk - percentage of iron material in disk. Imp in disk - percentage of impactor material in disk.

References

- [1] Melosh, H. A hydrocode equation of state for SiO₂. *Meteoritics & Planetary Science* **42**, 2079–2098 (2007).
- [2] Thompson, S. Aneos—analytic equations of state for shock physics codes, sandia natl. *Lab. Doc. SAND89-2951* (1990).
- [3] Canup, R. M. Forming a moon with an earth-like composition via a giant impact. *Science* **338**, 1052–1055 (2012).
- [4] Canup, R. M., Ward, W. R. & Cameron, A. A scaling relationship for satellite-forming impacts. *Icarus* **150**, 288–296 (2001).
- [5] Canup, R. M. Simulations of a late lunar-forming impact. *Icarus* **168**, 433–456 (2004).
- [6] Nakajima, M. & Stevenson, D. J. Investigation of the initial state of the moon-forming disk: Bridging SPH simulations and hydrostatic models. *Icarus* **233**, 259 – 267 (2014).
- [7] Wada, K., Kokubo, E. & Makino, J. High-resolution simulations of a moon-forming impact and postimpact evolution. *The Astrophysical Journal* **638**, 1180 (2006).
- [8] Canup, R. M. Dynamics of lunar formation. *Annual Review of Astronomy and Astrophysics* **42**, 441–475 (2004).
- [9] Salmon, J. & Canup, R. M. Accretion of the moon from non-canonical discs. *Philosophical Transactions of the Royal Society of London A: Mathematical, Physical and Engineering Sciences* **372** (2014).
- [10] Raymond, S. N., O’Brien, D. P., Morbidelli, A. & Kaib, N. A. Building the terrestrial planets: Constrained accretion in the inner solar system. *Icarus* **203**, 644 – 662 (2009).

- [11] Wisdom, J. & Tian, Z. Early evolution of the earth-moon system with a fast-spinning earth. *Icarus* **256**, 138 – 146 (2015).
- [12] Schlichting, H. E. & Sari, R. The effect of semicollisional accretion on planetary spins. *The Astrophysical Journal* **658**, 593 (2007).